RSC Advances

ROYAL SOCIETY OF CHEMISTRY

www.rsc.org/advances

Cite this: DOI: 10.1039/c0xx00000x

www.rsc.org/xxxxxx

ARTICLE TYPE

Facile Preparation of Novel Au-Polydopamine Nanoparticles Modified by 4-Mercaptophenylboronic acid for Glucose Sensor

Guohua Jiang,*[a,b,c] Tengteng Jiang,[a,b] Yuan Wang,[d] Xiangxiang Du,[a,b] Zhen Wei, [a,b] and Huijie Zhou[d]

Received (in XXX, XXX) Xth XXXXXXXXX 20XX, Accepted Xth XXXXXXXXX 20XX

DOI: 10.1039/b000000x

The Au nanoparticles (NPs) had been attached onto the surface of polydopamine (PDA) macrospheres by in-situ reduction reaction between PDA and $HAuCl_4$. And 4-mercaptophenyl boronic acid (MPBA) was further modified to Au-PDA composite particles via Au-S strong interaction. The resultant MPBA-Au-PDA particles were used to non-enzyme amperometric glucose sensor.

Glucose is a carbohydrate and the most important simple sugar in human metabolism. The normal concentration of glucose in the blood is about 0.1%, but it becomes much higher in persons suffering from diabetes. From a clinical perspective, a rapid, accurate, high sensitivity, low-cost and good reproducibility determination of glucose is particularly important in clinical diagnosing [1, 2]. Many efforts have been taken to monitor glucose concentrations in the human body. Among of them, enzyme-free electrochemical sensors have thus become a highly desirable project for glucose-sensor research due to the avoiding the use and sophisticated manufacture of GODx, are aimed at directly oxidizing the glucose in samples [3]. However, the poor measurement stability caused by surface poisoning from the intermediate products adsorbed and the effect of co-existing electro-active species are still the serious problems in the application of these electrochemical sensor materials.

The emergence and recent advance of nanomaterial science and nanotechnology provide new opportunities for enzyme-free glucose sensors. The nanomaterials of noble metals such as Pt[4], Pd[5] and Au[6]; non noble metals such as Cu [7] and Ni[8]; metal oxides such as Co_3O_4[9], Mn_xO_y[10] and Fe_xO_y[11]; and bimetallic composites[12] have been wildly used to produce novel electrochemical enzyme-free glucose sensors. In most cases, they involve using carbon materials as supporting materials to enhance the electron transfer ability and increase the surface area of the metal nanomaterials. For example, Pt nanoflower (PtNF) is synthesized on a SWCNTs film using electrodeposition. The as-prepared PtNF film exhibits excellent catalytic ability towards the amperometric detection of glucose at neutral pH [13]. Recently, Chen et al [14] prepared the PtNF and graphene oxide composites which showed a wide linear response for glucose from 2 μM to 20.3 mM.

Dopamine (3, 4-dihydroxyphenylethylamine) (DA), an important hormone and neurotransmitter, plays an important physiological role as a chemical messenger in mammalians. In the presence of dissolved O_2 and under alkaline conditions, aqueous solution of DA will spontaneously oxidize into polydopamine (PDA), yielding melanin-like polymer which can be deposited on both organic and inorganic surfaces [15]. Furthermore, PDA contains catechol functional groups, which makes it an efficient matrix for loading thiol- or amine-containing molecules through thiol- and amine-catechol adduct formation. Thus, this PDA functionalization provides an extremely versatile platform not only for the immobilization of biological molecules but also for the possible in situ deposition of metallic nanoparticles [16, 17]. The in situ deposition of high-content metallic NPs on the PDA not only provided a simple and controllable method for the nanoprobe preparation but also amplified the signal response of each immune-recognition event.

In the present work, PDA macrospheres were firstly prepared by polymerization of DA in the presence of F108 as a template surfactant under the alkaline conditions [18]. Due to the abundant of functional groups (-OH, $-NH_2$ on the surface of PDA spheres, they exhibited an extraordinary versatile active nature and had the abilities to reduce $AuCl_4$- ions to Au nanoparticles (NPs) [19]. The Au NPs had been attached onto the surface of PDA macrospheres by in-situ reduction reaction between PDA and $HAuCl_4$ to form Au-PDA composite particles. Then, 4-mercaptophenyl boronic acid modified Au-PDA composite particles (MPBA-Au-PDA) was prepared by via Au-S strong interaction. The resultant MPBA-Au-PDA particles were used to non-enzyme amperometric glucose sensor, as shown in Scheme 1 (see detail preparation in ESI).

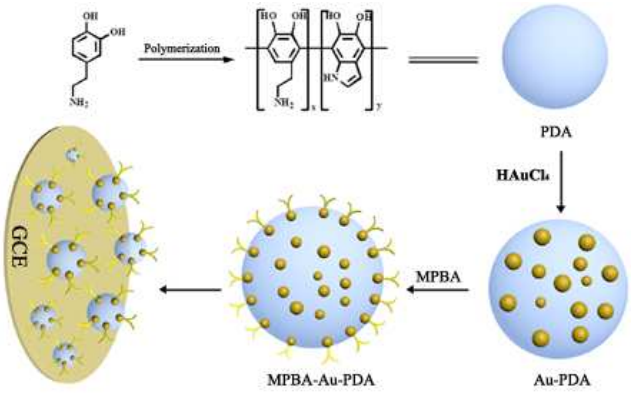

Scheme 1. Schematic illustration of the procedure for preparation of MPBA-Au-PDA modified glassy carbon electrode (GCE).

The PDA solution with black in color can be formed after the polymerization. The morphology and size of the PDA particles obtained in here (pH 8.0) was analyzed by scanning electron microscope (SEM) and transmission electron microscope (TEM) measurements (see Fig. S1 in ESI). The spherical particles with sizes of about 120 nm (Fig. 1A and 1B) can be founded which is consistent with the dynamic light scattering (DLS) result at 123.4 nm (see Fig. S2 in ESI). Due to the reduction ability and metal binding affinity of the catechol groups of PDA [20], $HAuCl_4$ was reduced into Au NPs which endowed the reactive solution with a golden color, and these Au NPs are immobilized on the surface of PDA (see Fig. S3 in ESI). As shown in Fig. 1C, the size of Au NPs with less than 10 nm can be observed. The typical HRTEM image (insert in Fig. 1C) with clear lattice fringes having a spacing of about 0.25 nm revealed that the growth of Au NPs occurred preferentially on the (111) plane [21]. Electron diffraction pattern of Au-PDA exhibits the diffraction rings with non-continuous but spotty (Fig. 1D), indicating that some grains of the hydride phases during the formation process of Au NPs.

The XRD patterns of the as-synthesized PDA and Au-PDA are shown in Fig. 2A. Because of the amorphous crystallinity of the PDA, the obvious diffraction peak at 20° for the PDA can be observed [22]. The crystal structure of the as-prepared Au-PDA hybrid was also confirmed by means of XRD characterization (Fig. 2A). Except from the diffraction peak of PDA, the major diffraction peaks at the Bragg angles of 38.4°, 44.4°, 64.8° and 77.8° and 81.9° were observed, which can be indexed to the (111), (200), (220) and (311) reflections of face-centered cubic (fcc) phase of metallic gold (JCPDS, card no. 04-0784), showing the crystalline nature of the particles [23]. The results also indicated that the Au NPs were produced in a well-dispersed way on the PDA particles. The average size of the Au NPs is 9.63 nm, calculated by the Scherrer formula (see calculation in ESI), which is in good agreement with the results from the TEM image. By utilizing the specific Au-S strong interaction, MPBA molecules can be introduced onto the surface of Au NPs to form MPBA-Au-PDA hybrid and the linkage was confirmed by infrared spectra, as shown in Fig. 2B. The PDA had a broad peak around 3400 cm^{-1} ascribed to aromatic -NH_x and -OH stretching vibrations. It also presented peaks at 2920 cm^{-1} and 2850 cm^{-1} (C-H stretching vibrations), 1600 cm^{-1} (the overlap of C=C resonance vibrations in aromatic ring) and 1510 cm^{-1} (N-H scissoring vibrations) [24]. Interesting, after modification by Au and MBPA, peaks at 3400 cm^{-1} and 1601 cm^{-1} were become narrower with reduced peak intensity due to the oxidation of -NH_x during the formation of Au NPs. And two new strong peaks at 1390 and 1350 cm^{-1} ascribed to B-O stretching vibrations of boronic acid in MPBA can be observed [25]. The EDS technique was further used to verify the presence of Au and MPBA in the Au-PDA and MPBA-Au-PDA systems, respectively. It is found that the C, O and Au atoms are in the Au-PDA. After modification by MPBA, a new S atomic signal from the thiol of MPBA can be observed, as shown in Fig. 2C.

Fig. 3A shows the cyclic voltammograms (CVs) in 0.1 mol/L PBS in potential range of -0.6 to 0.6 V with the scan rate from 20 to 500 $mV \cdot s^{-1}$ at MBPA-Au-PDA electrode. As expected, the voltammograms had well-defined redox peaks, and the peak currents increased gradually with the increase of the scan rates. Fig. 3B shows the relationship between peak current and square root of scan rate obtained from the experimental data in Fig. 3A. The anodic and cathodic peak currents both show linear dependence on the square root of the scan rate. The linear regression equations were as follows: $Ipc = 0.2029V^{1/2}+0.24306$, $R = 0.99745$; $i_{pa} = -0.27848\ V^{1/2}+ 0.06087$, $R = 0.99962$. This deviation from a linear relationship suggests that the redox reaction of MBPA-Au-PDA is a surface-controlled process, not a diffusion-controlled process [26]. The pH of electrolyte can effect on the stability of MBPA-Au-PDA electrode, which has been reported in many papers [20]. In present work, the electrochemical response of MBPA-Au-PDA was examined in 0.1 mol/L PBS solutions at various pH. As shown in Fig. 3C, with the increasing pH value, the redox peak potential barely changed, indicating that no proton is involved in the electrochemical reaction of MBPA. Interestingly, although the peak current had the tendency to decrease, it actually changed slightly, implying the working electrode can be used in wide pH range. It is probable that Au NPs and PDA have favored the stability of MBPA. The boronic acid usually has a high pK_a around 8.2 [27, 28], while the boronate ester shows higher acidity (pK_a 6.0). Thus a pH value near physiological of 7.0 was utilized in the experiments. For further characterization of the modified electrode, electrochemical impedance spectroscopy (EIS) was used. EIS is also a highly effective method for probing the features of a surface-modified

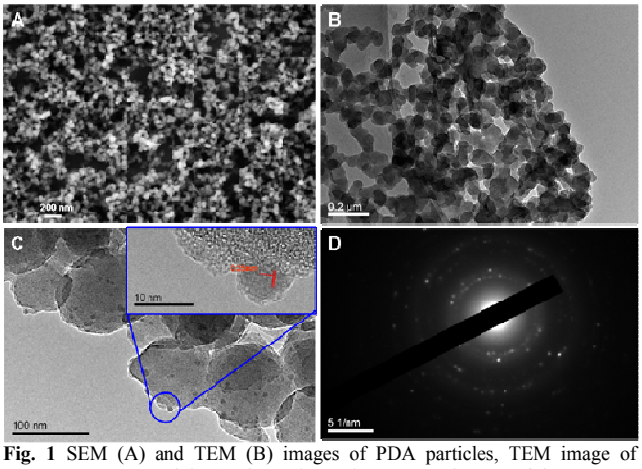

Fig. 1 SEM (A) and TEM (B) images of PDA particles, TEM image of MPBA-Au-PDA particles (C, inset shows the HRTEM images of the Au NPs) and electron diffraction pattern of a nano-sized region containing Au NPs.

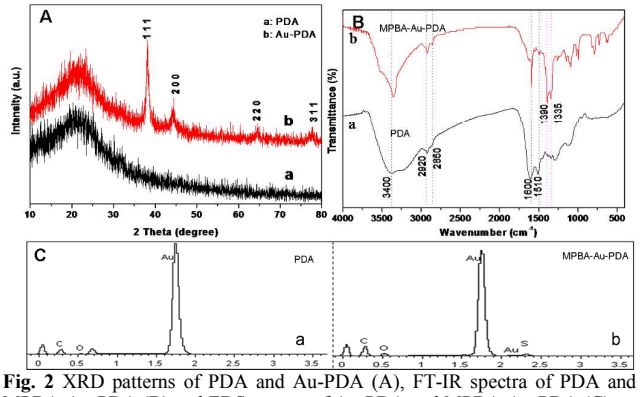

Fig. 2 XRD patterns of PDA and Au-PDA (A), FT-IR spectra of PDA and MPBA-Au-PDA (B) and EDS spectra of Au-PDA and MPBA-Au-PDA (C).

electrode. In EIS, the semicircle diameter of impedance equals the electron transfer resistance (R_{et}), which controls the electron transfer kinetics of the redox probe at the electrode surface [3]. Fig. 3D shows Nyquist plots of bare glassy carbon electrode, Au-PDA and MPBA-Au-PDA modified electrodes with 0.1mol/L KCl and 5.0 mmol/L $K_3[Fe(CN)_6]$. The bare GCE (curve a) displayed a small semi-circle with a R_{et} of about 300 Ω at high frequencies. After the bare electrode was modified with Au-PDA hybrid, the electrode showed a much lower resistance for the redox probe (curve b), implying that Au-PDA hybrid was an excellent electric conducting material and accelerated the electron transfer. After the electrodes modified by MPBA-Au-PDA, the Nyquist plots of the MPBA-Au-PDA modified electrode consist of a semicircle at high frequency and a straight line at low frequency. The R_{et} increased significantly to about 2000 Ω (curve c), which indicated the formation of complex layer embarrassed the electron transfer. The middle frequency semicircle is attributed to the charge transfer, and the low frequency line to the ion diffusion. These results were consistent with those obtained in CV.

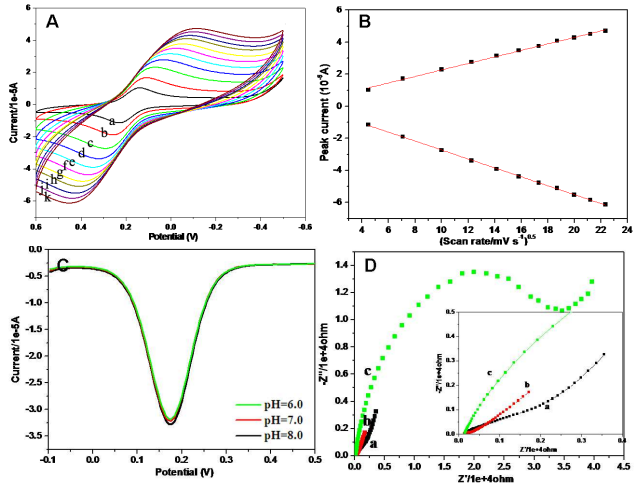

Fig. 3 CV curves of MBPA-Au-PDA in 0.1mol/L PBS with different scan rates (a: 20, b: 50, c: 100, d: 150, e: 200, f: 250, g: 300, h: 350, i: 400, j: 450, k: 500 mVs^{-1}) (A), the relations of peak current versus the square root of scan rate (B), DPVs of the MPBA-Au-PDA in 0.1 mol/L PBS at various pH (green: pH=6, red: pH=7 and black: pH=8) and concentration of D-glucose controlled at 6.0 mmol/L (C) and Nyquist plots of (a: the bare glassy carbon electrode, b: Au-PDA and c: MPBA-Au-PDA) with 0.1 mol/L KCl and 5.0 mmol/L $K_3[Fe(CN)_6]$ (D).

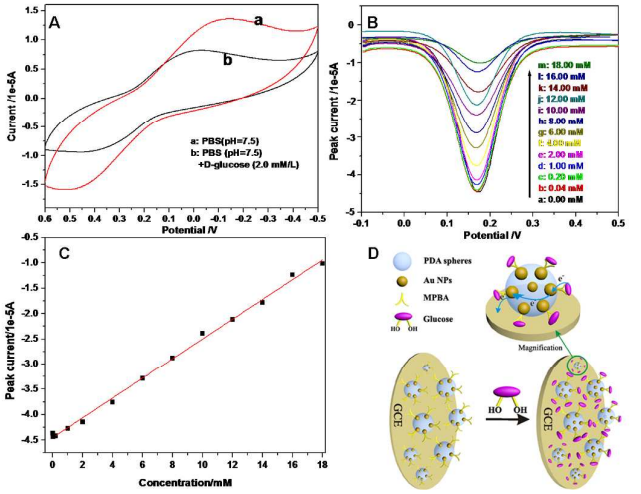

Fig. 4 CVs of MPBA-Au-PDA modified electrodes in 0.1mol/L PBS (pH = 7.0) at a scan rate of 50 mV s^{-1} (a) and with concentration of D-glucose at 2mmol/L (b) (A). DPVs of MPBA-Au-PDA in 0.1 mol/L PBS at pH = 7 and the concentration of D-glucose increasing from 0 to 18 mmoL/L (a: 0.00, b: 0.04, c: 0.20, d: 1.00, e: 2.00, f: 4.00, g: 6.00, h: 8.00, i: 10.00, j: 12.00, k: 14.00, l: 16.00, m: 18.00 mM) (B), the linear relationship between the peak current and the concentration of D-glucose (C) and the mechanism of the binding between MPBA and D-glucose (D).

Upon addition of glucose, MPBA would react with the 1, 2-diol of D-glucose to form a stable 5-membered cyclic boronate ester. A non enzyme based amperometric glucose sensor was fabricated with MPBA-Au-PDA as the electrochemical indicator. The decreased peak current should be proportional to the concentration of D-glucose (Fig. 4A). Fig. 4B shows the DPV responses of MPBA-Au-PDA modified electrodes to different concentrations of D-glucose solution (0.1 M PBS, pH=7.0) in range of 0~18 mmoL/L. One can observe the peak current decreased with increasing the concentration of D-glucose from 0 to 18 mmoL/L. The regression equation was expressed as: $Y=-4.453\times10^{-5} + 1.952\times10^{-6}$ C (mmol/L), R = 0.9953, as shown in Fig. 4C. A detection limit of 5.0×10^{-8} M was estimated using 3σ method (see calculation in ESI). Compared the other glucose sensors [29-34], the present sensor possessed wide linear range, high sensitivity, low detection limit and excellent reproducibility. For example, C_{60}-$TOAB^+$ composite for glucose detection [34] exhibited a linear response range from 500 nM to 13 mM and a detection limit at 1.67×10^{-7} M. Although the proposed sensor possessed a linear range which is not in the realm of blood sugar level, it can be used in real sample analysis just by diluting the sample. As shown in Fig. 4D, the binding between MPBA and D-glucose obstructed the diffusion of ions across the composite matrix as well as the electron transfer, which was reflected by the decreased peak current.

Conclusions

In summary, a novel MPBA modified Au NPs that in situ deposition on PDA microspheres was prepared for the ultrasensitive non-enzymatic electrochemical immunoassay for glucose. This in-situ deposition method provides a simple and controllable way to prepare a novel glucose sensor. The proposed immobilization strategy provides a useful platform for electrochemical immunoassay for wide-range glucose concentration and could be readily extended toward the on-site monitoring of glucose in the blood for diabetes in clinical diagnosing. This approach is simple, inexpensive, quick, and "green". In addition, due to the good chemical stability, excellent hydrophilic and biocompatible properties of PDA, the design and synthesis of multi-functional PDA-based bio-nanocomposites with interesting properties has been proven to be an efficient approach for the construction of high performance biosensing.

Acknowledgements

This work wad financially supported by the National Natural Science Foundation of China (51373155), "521 Talents Training Plan" in Zhejiang Sci-Tech University (ZSTU) and National Training Programs of Innovation and Entrepreneurship for Undergraduates (H. Zhou).

Notes and references

[a] *Department of Materials Engineering, Zhejiang Sci-Tech University, Hangzhou 310018, P. R. China. Tel: +86 571 86843527; E-mail address: ghjiang_cn@zstu.edu.cn (G. Jiang)*
[b] *National Engineering Laboratory for Textile Fiber Materials and Processing Technology (Zhejiang), Hangzhou 310018, P. R. China.*
[c] *Key Laboratory of Advanced Textile Materials and Manufacturing Technology (ATMT), Ministry of Education, Hangzhou 310018, P. R. China.*
[d] *Qixin Honours School, Zhejiang Sci-Tech University, Hangzhou 310018, P. R. China.*

† Electronic Supplementary Information (ESI) available: details of materials, synthesis of PDA microspheres, preparation of Au-PDA microspheres, preparation of MPBA-Au-PDA nanocomposites, characterization, calculation of the size of Au NPs and calculation of LOD. See DOI: 10.1039/b000000x/

1 G. Jiang, T. Jiang, X. Li, Z. Wei, X. Du, X. Wang, *Mater. Res. Express*, 2014, 1, 025708.
2 T. Jiang, G. Jiang, X. Wang, Y. Dong, Z. Wei, X. Li, B. Tang, Des. Monomers Polym., 2014, 17, 576-581.
3 Z. Wang, K. Shang, J. Dong, Z. Cheng, S. Ai, *Microchim. Acta*, 2012, 179, 227-234.
4 L. Xu, Y. Zhu, L. Tang, X. Yang, C. Li. *Electroanalysis*, 2007, 19, 717-722.
5 C. Yang, X. Zhang, G. Lan, L. Chen, M. Chen, Y. Zeng, J. Jiang. *Chin. Chem. Lett.*, 2014, 25, 496-500.
6 Y. Wu, S. Hu. *Bioelectrochemistry*, 2007, 70, 335-341.
7 X. Kang, Z. Mai, X. Zou, P. Cai, J. Mo. *Chin. Chem. Lett.*, 2007, 18, 189-191.
8 M. Yousef Elahi, H. Heli, S. Z. Bathaie, M. F. Mousavi. *J. Solid State Electrochem.*, 2007, 11, 273-282.
9 C. Hou, Q. Xu, L. Yin, X. Hu. *Analyst*, 2012, 137, 5803-5808.
10 J. Yu, S. Hu. *Electrochim. Acta*, 2010, 55, 3471-3476.
11 S. Masoomi-Godarzi, A. A. Khodadadi, M. Vesali-Naseh, Y. Mortazavi. *J. Electrochem. Soc.*, 2014, 161, 19-25.
12 X. Cao, N. Wang, S. Jia, Y. Shao. *Anal. Chem.*, 2013, 85, 5040-5046.
13 L. Su, W. Jia, L. Zhang, C. Beacham, H. Zhang, Y. Lei, *J. Phys. Chem. C*, 2010, 114, 18121-18125.
14 G. Wu, X. Song, Y. Wu, X. Chen, F. Luo, X. Chen, *Talanta*, 2013, 105, 379-385.
15 F. Li, L. Yang, C. Zhao, Z. Du, F. Luo, X. Chen, *Anal. Methods*, 2011, 3, 1601-1606.
16 K. Jia, M. Khaywah, Y. Li, J. Bijeon, P. Adam, R. Déturche, B. Guelorget, M. François, G. Louarn, R. Ionescu, *ACS Appl. Mater. Interfaces*, 2014, 6, 219-227.
17 M. Sureshkumar, P. -N. Lee, C. -K. Lee, *J. Mater. Chem.*, 2011, 21, 12316-12320.
18 J. Yan, L. Yang, M. -F. Lin, J. Ma, X. Lu, P. Lee, *Small*, 2013, 9, 596-603.
19 Z. Ma, X. Jia, J. Hu, F. Zhou, B. Dai, RSC Adv., 2014, 4, 1853-1856.
20 J. Li, Z. Wang, P. Li, N. Zong, F. Li, *Sensors and Actuators B*, 2012, 161, 832-837.
21 Y. Miao, H. Ascolani, G. Zampieri, D. Woodruff, C. Satterley, J. Robert, V. Dhanak, *J. Phys. Chem. C*, 2007, 111, 10904-10914.
22 M. Zhang, X. He, L. Chen, Y. Zhang, *J. Mater. Chem.*, 2010, 20, 10696-10704.
23 R. Liang, X. Meng, C. Liu, J. Qiu, *Electrophoresis*, 2011, 32, 3331-3340.
24 R. Luo, L. Tang, S. Zhong, Z. Yang, J. Wang, Y. Weng, Q. Tu, C. Jiang, N. Huang. *ACS Appl. Mater. Interfaces*, 2013, 5 , 1704-1714.
25 A. Kawamoto, L. Pardini, M. Diniz, V. Lourenco, M. Takahashi, *J. Aerosp. Technol. Manag.*, 2010, 2, 169-182.
26 Y. Zhu, C. Wang, *J. Phys. Chem. C*, 2011, 115, 823-832.
27 Z. Xu, K. Uddin, T. Kamra, J. Schnadt, L. Ye, *ACS Appl. Mater. Interfaces*, 2014, 6, 1406-1414.
28 B. Kumar, K. Salikolimi, M. Eswaramoorthy, *Langmuir*, 2014, 30, 4540-4544.
29 X. Xiao, M. Wang, H. Li, Y. Pan, P. Si. *Talanta*, 2014, 125, 366-371.
30 T. Alizadeh, S. Mirzagholipur. *Sensor Actuat B-Chem.*, 2014, 198, 438-447.
31 E. Sharifi, A. Salimi, E. Shams, A. Noorbakhsh, M. K. Amini. *Biosens Bioelectron.*, 2014, 56, 313-319.
32 Y. Li, X. Niu, J. Tang, M. Lan, H. Zhao. *Electrochim. Acta*, 2014, 130, 1-8.
33 K. Dhara, J. Stanley, T. Ramachandran, B. G. Nair, S. Babu. *Sensor Actuat B-Chem.*, 2014, 195, 197-205.
34 C. Ye, X. Zhong, R. Yuan, Y. Chai. *Sensor Actuat B-Chem.*, 2014, 199, 101-107.

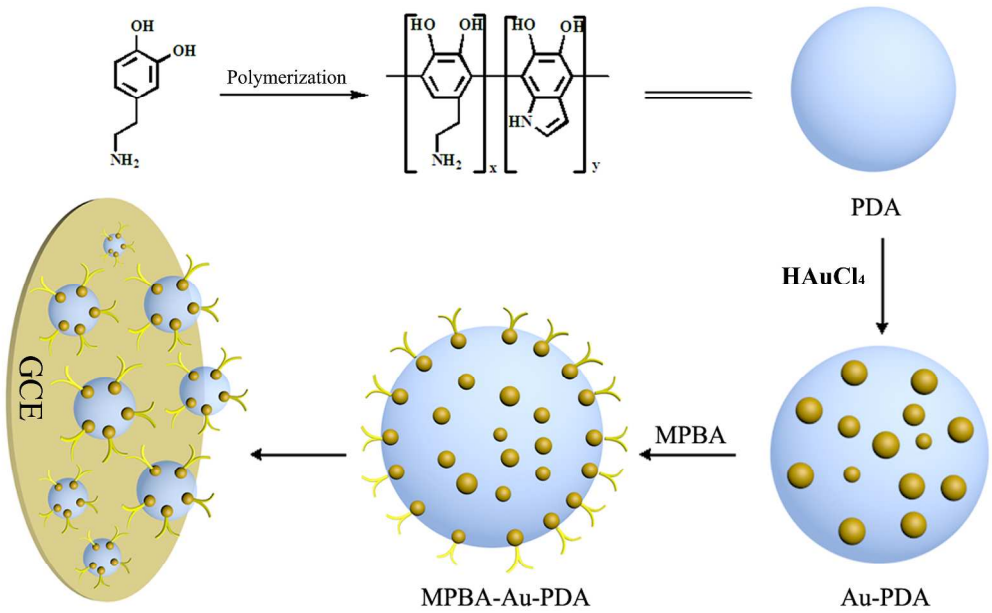

Scheme 1. Schematic illustration of the procedure for preparation of MPBA-Au-PDA modified glassy carbon electrode (GCE).

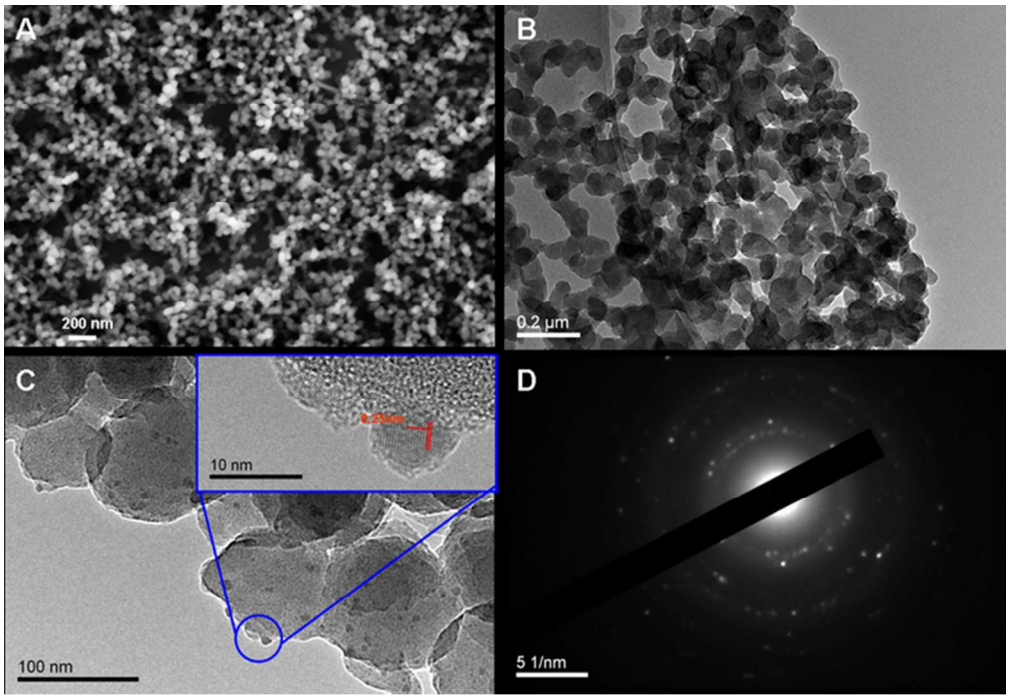

Fig. 1 SEM (A) and TEM (B) images of PDA macrospheres, TEM image of MPBA-Au-PDA particles (C, inset shows the HRTEM images of the Au NPs) and electron diffraction pattern of a nano-sized region containing Au NPs.
61x42mm (300 x 300 DPI)

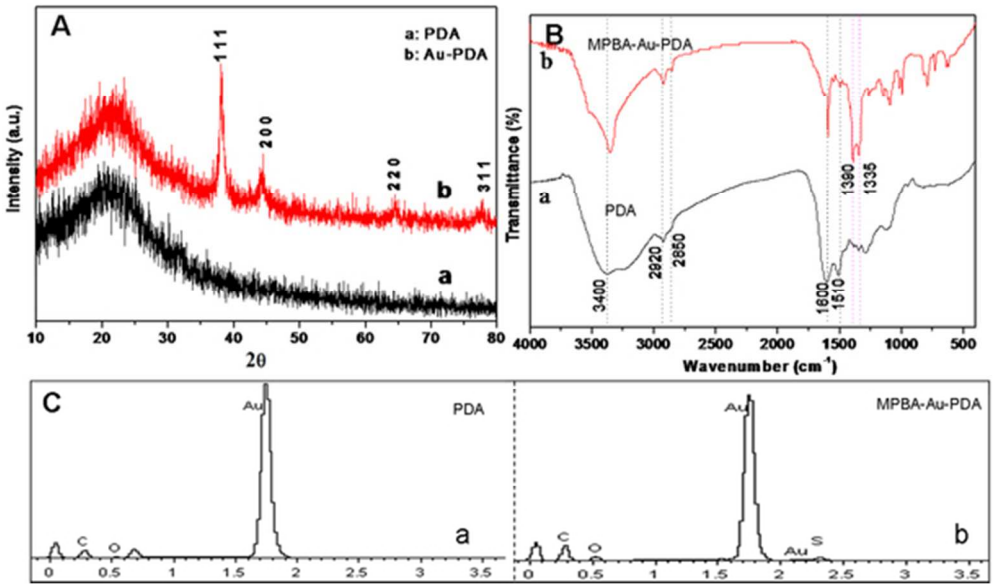

Fig. 2 XRD patterns of PDA and Au-PDA (A), FT-IR spectra of PDA and MPBA-Au-PDA (B) and EDS spectra of Au-PDA and MPBA-Au-PDA (C).
51x30mm (300 x 300 DPI)

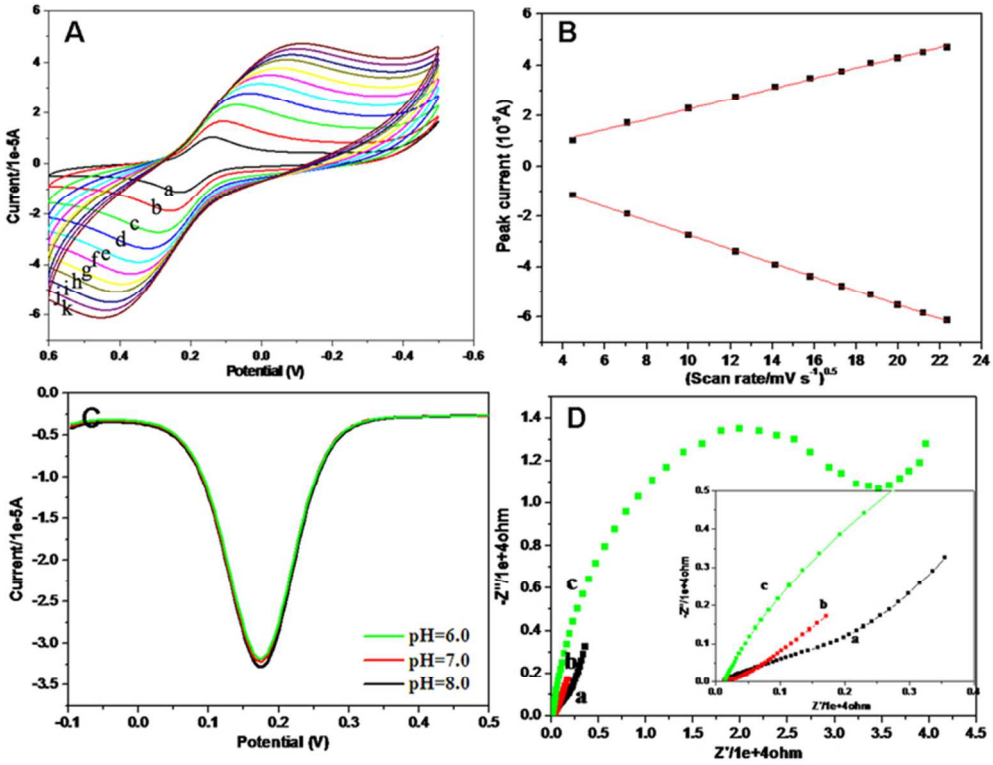

Fig. 3 CV curves of MBPA-Au-PDA in 0.1mol/L PBS with different scan rates (a: 20, b: 50, c: 100, d: 150, e: 200, f: 250, g: 300, h: 350, i: 400, j: 450, k: 500 mVs-1) (A), the relations of peak current versus the square root of scan rate (B), DPVs of the MPBA-Au-PDA in 0.1 mol/L PBS at various pH (green: pH=6, red: pH=7 and black: pH=8) and concentration of D-glucose controlled at 6.0 mmol/L (C) and Nyquist plots of (a: the bare glassy carbon electrode, b: Au-PDA and c: MPBA-Au-PDA) with 0.1mol/L KCl and 5.0 mmol/L K3[Fe(CN)6] (D).
68x52mm (300 x 300 DPI)

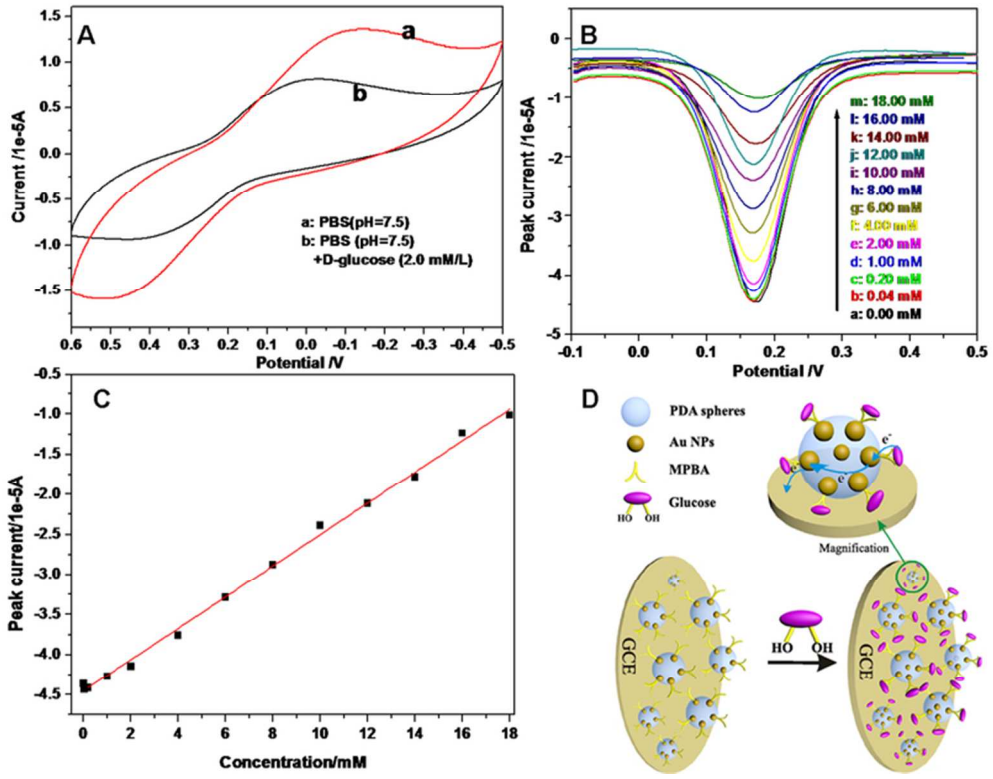

68x53mm (300 x 300 DPI)

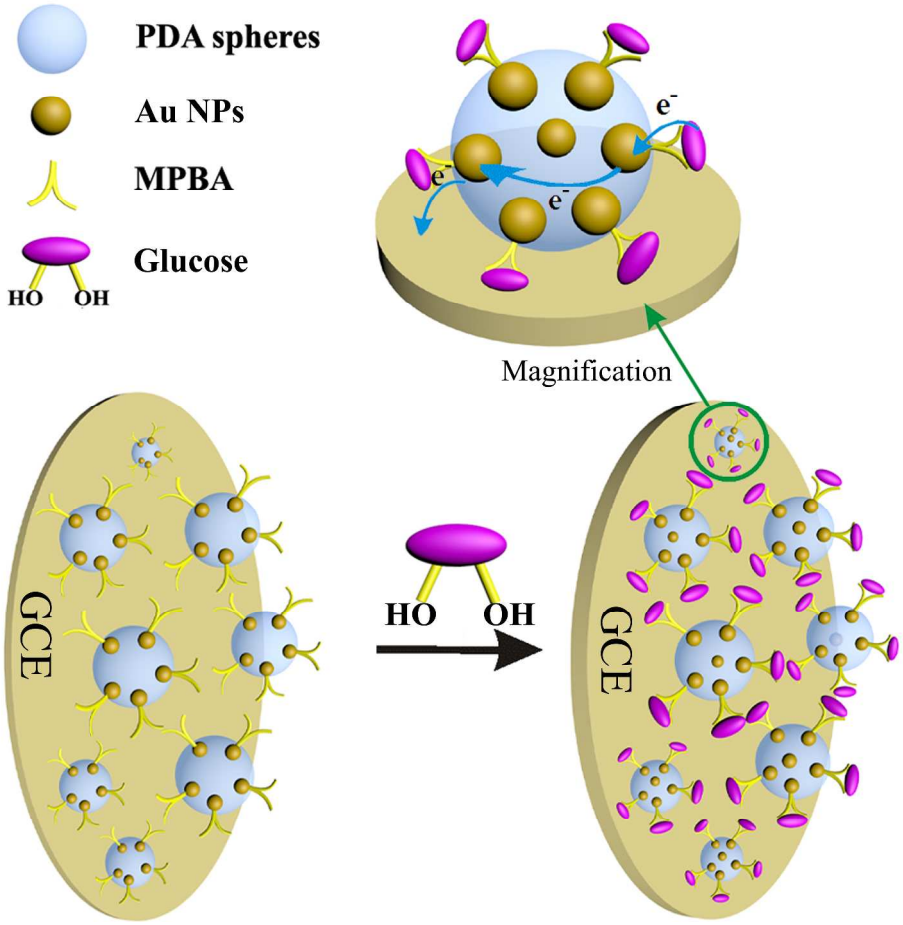

MPBA-Au-PDA composite particles were prepared for the ultrasensitive non-enzymatic electrochemical immunoassay for glucose.